PERGAMON

Planetary and Space Science 49 (2001) 1481–1500

Planetary and Space Science

www.elsevier.com/locate/planspasci

# The MESSENGER mission to Mercury: spacecraft and mission design

Andrew G. Santo[a,*], Robert E. Gold[a], Ralph L. McNutt, Jr.[a], Sean C. Solomon[b], Carl J. Ercol[a], Robert W. Farquhar[a], Theodore J. Hartka[a], Jason E. Jenkins[a], James V. McAdams[a], Larry E. Mosher[a], David F. Persons[a], David A. Artis[a], Robert S. Bokulic[a], Richard F. Conde[a], George Dakermanji[a], Milton E. Goss, Jr.[a], David R. Haley[a], Kenneth J. Heeres[a], Richard H. Maurer[a], Robert C. Moore[a], Elliot H. Rodberg[a], Theodore G. Stern[c], Samuel R. Wiley[d], Bobby G. Williams[e], Chen-wan L. Yen[e], Max R. Peterson[a]

[a] *The Johns Hopkins University Applied Physics Laboratory, Laurel, MD 20723, USA*
[b] *Department of Terrestrial Magnetism, Carnegie Institution of Washington, Washington, DC 20015, USA*
[c] *Composite Optics Incorporated, 9617 Distribution Avenue, San Diego, CA 92121, USA*
[d] *GenCorp Aerojet, PO Box 13222, Sacramento, CA 95813-6000, USA*
[e] *Jet Propulsion Laboratory, California Institute of Technology, Pasadena, CA 91109, USA*

Received 2 November 2000; accepted 18 January 2001

**Abstract**

A Mercury orbiter mission is challenging from thermal and mass perspectives. The Mercury Surface, Space Environment, Geochemistry, and Ranging (MESSENGER) mission overcomes these challenges while avoiding esoteric technologies by using an innovative approach with commonly available materials, minimal moving parts, and maximum heritage. This approach yields a spacecraft with good margins in all categories and low technical risk. The key concepts are a ceramic-cloth sunshade, an integrated lightweight structure and high-performance propulsion system, and a solar array incorporating optical solar reflectors (OSRs). The sunshade maintains the spacecraft at room temperature. The integrated structure and propulsion system provides ample mass margin. The solar array with OSRs, which has already undergone significant testing, provides thermal margin even if the panels are inadvertently pointed directly at the Sun at 0.3 AU.


## 1. Introduction

Mercury is the least characterized of the terrestrial planets, yet it holds unique clues to questions of planet formation, geological and interior evolution, magnetic field generation, magnetospheric physics, and volatile inventories in the inner solar system (Solomon et al., 2001). The planet has been visited by only a single spacecraft, Mariner 10, which flew by Mercury three times in 1974–1975 (Dunne and Burgess, 1978). While a Mercury orbiter was widely recognized as the obvious next step in the exploration of the planet, in the decade following Mariner 10 it was generally thought that insertion of a spacecraft into orbit around Mercury could not be achieved by a conventional propulsion system. With the recognition that gravity-assisted trajectories using conventional launch systems now permit the insertion of a spacecraft into Mercury orbit (Yen, 1985, 1989), the need for the intensive exploration of the innermost planet has been recognized in the plans of the National Aeronautics and Space Administration (NASA, 1997; Roadmap Development Team, 1998). Partly in response to this priority, the Mercury Surface, Space Environment, Geochemistry, and Ranging (MESSENGER) mission was selected under NASA's Discovery Program in July 1999.

The scientific objectives for the MESSENGER mission, described in a companion paper (Solomon et al., 2001), dictate a set of measurement requirements that will be met by a payload of seven scientific instruments. Characteristics of these instruments are given in a second accompanying paper (Gold et al., 2001).

The MESSENGER mission is led by the Carnegie Institution of Washington and The Johns Hopkins University Applied Physics Laboratory (JHU/APL). Consortium team members include Composite Optics, Inc., a leader in light-weight spacecraft structures, GenCorp Aerojet, a leader in spacecraft propulsion systems, the NASA Goddard Space

* Corresponding author. Tel.: +1-240-228-6120; fax: +1-240-228-6635.
*E-mail address:* andy.santo@jhuapl.edu (A.G. Santo).

0032-0633/01/$ - see front matter 
PII: S0032-0633(01)00087-3

Table 1
MESSENGER mission design summary

| | | |
|---|---|---|
| Two launch opportunities | March 10–29, 2004 (20 days)<br>May 12–23, 2004 (12 days) | |
| Mission duration | 6.1 y (1-y orbit phase) | |
| Orbit type | Mercury orbit (inclined elliptical) | |
| Orbital parameters (Mercury orbit phase) | Semimajor axis | 10,136 km |
| | Eccentricity | 0.7396 |
| | Inclination | 80° |
| | Longitude of ascending node | 316° |
| | Argument of periapsis | 118° |
| Launch vehicle | Delta 2925H–9.5 | |
| Launch energy | $C_3 = 14.8$–$17.8\ km^2/s^2$ | |
| Launch mass (99% PCS) | $M_0 = 1093$ kg | |
| Heliocentric spacecraft distances | Max 1.01 AU, min 0.30 AU | |
| $\Delta V$ budget | 2300 m/s (110 m/s margin) | |

Flight Center, the University of Colorado, and the University of Michigan. Co-engineered with planetary-science specialists from twelve institutions, MESSENGER is being designed to accommodate the severe near-Sun thermal environment and supply the necessary large spacecraft velocity changes while enabling all required science observations. This paper describes the principal elements of mission and spacecraft design at this stage of preparation for the MESSENGER mission.

## 2. Mission design

MESSENGER's trajectory begins with launch on March 10, 2004, and continues with unpowered gravity assists from Venus (twice) and Mercury (twice). MESSENGER enters Mercury orbit on April 6, 2009. The cruise phase offers opportunities for early science at the Mercury and Venus flybys. The Mercury orbital phase lasts one Earth-year (4.2 Mercury yr). The total mission $\Delta V$ budget is 2300 m/s. Table 1 summarizes the mission design.

### 2.1. Mission design overview

Trajectory optimization for a Delta 2925H-9.5 launch vehicle yields 20-day baseline and 12-day backup launch periods in March and May of 2004. A further opportunity in August 2005 also exists (Yen, 1985, 1989; McAdams et al., 1998). The launch energy ($C_3$) requirement is less than $18.0\ km^2/s^2$ for all launch periods, and the deterministic $\Delta V$ varies between 2001 and 2084 m/s. After launch from the Eastern Test Range, MESSENGER is delivered into a 185-km-altitude, 28.5°-inclination parking orbit before injection into the heliocentric transfer orbit.

An ecliptic-plane projection of the heliocentric trajectories and a key-event timeline are displayed in Fig. 1. The heliocentric trajectory begins with an Earth-to-Venus transfer and a Venus flyby on June 24, 2004. While Venus orbits the Sun 2.8 times, the spacecraft orbits the Sun 3.7 times enroute to a Venus flyby on March 16, 2006. The initial Venus flyby reduces aphelion to 0.78 AU and helps align the spacecraft orbit plane with Mercury's orbit plane. The second Venus flyby further aligns the orbit plane of the spacecraft with Mercury and also lowers orbit perihelion to 0.33 AU. The second Venus flyby occurs 3.4 orbits of the Sun before the spacecraft encounters Mercury. Mercury flybys include 200-km altitude, dark-side close approaches on July 21, 2007, and April 11, 2008. A deep-space maneuver (DSM) follows each Mercury flyby; both target the spacecraft for the next Mercury encounter. Flyby minimum altitudes, velocities, and phase angles are shown in Table 2. The phase angle describes the Sun-viewing geometry of the flyby. It is defined as the angle between the Sun, planet, and spacecraft. The heliocentric-phase mission design solution was verified by programs from Adasoft, Science Applications International Corporation, and NASA/Jet Propulsion Laboratory (JPL).

During the heliocentric phase there are several periods of solar conjunction, during which communications are limited while the spacecraft, Earth, and Sun are aligned within 2°. The two longest solar conjunctions, which last 11 (September 28–October 9, 2004) and 6 days (August 20–August 26, 2005), occur at least three months from any major event. A 3-day solar conjunction will occur as the spacecraft nears Mercury orbit insertion (MOI), but careful planning will reduce navigational uncertainties, and the risk to the mission design is manageable. Prior to the start of the 11- and 6-day conjunction periods the spacecraft is put into a safe state. During these conjunction periods, no time-triggered commands are executed. The spacecraft controls momentum through off-pointing to avoid momentum dumping and awaits commands from the ground.

At Mercury arrival the spacecraft performs an orbit-insertion maneuver to establish a 12-h, 200-km by 15,193-km-altitude orbit inclined 80° to Mercury's equator (Fig. 2). Mercury does not obstruct the Earth-spacecraft line of sight (Earth occultation) during MOI. The 93.3° approach phase angle and near-polar orbit set the initial orbit orientation nearly over the dawn–dusk terminator. The maximum eclipse period during orbital operations is 60 min. The periapsis latitude drifts from 60.0°N to 73.9°N, and orbit inclination varies from 80.0° to 81.6° during the one Earth-year of orbit operations. During November 2009, spacecraft communications will not be possible during a 6-day solar conjunction. This will be the only solar conjunction lasting more than three days during Mercury orbit. Prior to this conjunction period, as in the heliocentric-phase cases, the spacecraft is put into a safe state and awaits commands from the ground.

The parameters of the near-polar orbit provide maximum science return when considering thermal, power, communication, and propulsion constraints. The orbital-phase instru-

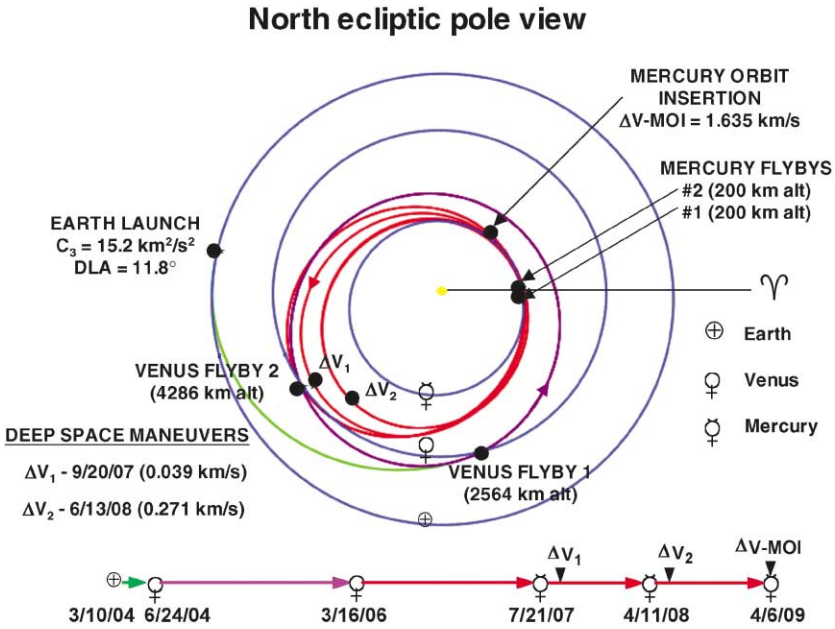


Fig. 1. The MESSENGER heliocentric orbit, shown projected onto the ecliptic plane, employs two Venus and two Mercury flybys (see timeline at bottom) to reduce the orbital energy to a point where a chemical-propulsion solution is feasible. This orbit solution is an improvement on the original Mercury orbiter ballistic trajectory solutions developed in the 1980s. Even with the benefits of the new mission design, propellant constitutes 57% of the spacecraft mass at launch.

Table 2
Flyby characteristics

| Flyby event | Date | Min. altitude (km) | Velocity (km/s) | Phase angle (°) |
|---|---|---|---|---|
| Venus #1 | June 24, 2004 | 2564 | 8.1 | 162 |
| Venus #2 | March 16, 2006 | 4286 | 8.1 | 33 |
| Mercury #1 | July 21, 2007 | 200 | 5.8 | 110 |
| Mercury #2 | April 11, 2008 | 200 | 5.5 | 127 |

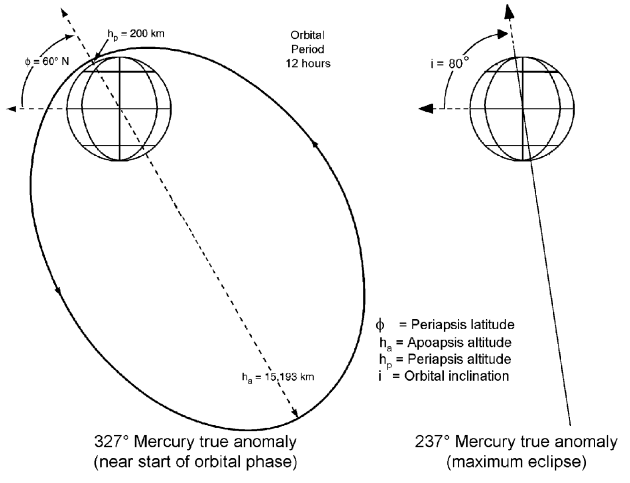


Fig. 2. The MESSENGER orbit around Mercury was chosen as a compromise between science viewing opportunities and spacecraft engineering difficulty. Periapsis latitude and altitude were balanced against the design of the spacecraft thermal and power systems.

ment observation sequence and timeline are contained in an accompanying paper (Solomon et al., 2001). The 12.0-h orbit period enables regular mission operations scheduling and maximizes time available to downlink science data around apoapsis. The first periapsis altitude after MOI is 200 km. This configuration is well within thermal design constraints because the initial orbit is in the dawn–dusk terminator and the sub-periapsis point moves into the night hemisphere. Periapsis altitude continues to rise over the rest of the mission due to solar perturbations. Every 88 days, one Mercury year, a two-burn sequence is executed to reduce the periapsis back to 200 km and adjust the orbit period to 12 h. The periapsis altitudes at the end of the first three Mercury years, prior to the orbit-adjust maneuvers, are 465, 437, and 402 km, respectively. After the last maneuver, at the end of the third Mercury year, the orbit is not adjusted further. At the end of the mission, 4.2 Mercury years after MOI, the periapsis altitude is 413 km. To meet navigation and science measurement objectives, ranging is performed for 30 min near periapsis and apoapsis every 5–10 orbits.

The $\Delta V$ allocation is shown in Table 3. The cleanup of execution errors is calculated at a 99% probability level ($\Delta V_{99}$), under the assumption of 1% spherical maneuver execution errors ($1\,\sigma$). The MOI maneuver includes a periapsis rotation from 62.3° to 60.0°N. Small $\Delta V$ burns ($\ll 1$ m/s) are executed approximately every fourth day during the orbital phase to manage spacecraft momentum. The mission is designed so that all $\Delta V$s inside 0.7 AU are executed with the sunshade protecting the spacecraft from solar illumination.

Table 3
$\Delta V$ allocation

| Category | | $\Delta V$(m/s) |
|---|---|---|
| *Deterministic* | | 2020 |
| Deep Space Maneuvers | 310 | |
| Mercury Orbit Insertion (MOI) | 1514 | |
| MOI finite burn penalty | 121 | |
| Orbit Maintenance (1-yr) | 75 | |
| *Statistical* | | 280 |
| Navigation ($\Delta V_{99}$) and attitude control | 170 | |
| Margin | 110 | |
| *Total* | | 2300 |
| Monopropellant ($N_2H_4$)$\Delta V$ | 233 | |
| Bipropellant ($N_2H_4 + N_2O_4$)$\Delta V$ | 2067 | |

### 2.2. Navigation

A preliminary navigation accuracy analysis has shown that the planned Deep Space Network (DSN) tracking coverage for the MESSENGER mission design provides sufficient navigation performance and margin throughout all mission phases. The navigation strategy for MESSENGER includes moderate DSN tracking for quiet cruise periods and additional tracking near critical events such as launch, gravity-assist flybys of Venus and Mercury, and propulsive maneuvers. This strategy relies on fitting longer arcs (up to 3.5 months) of tracking and characterizing the spacecraft non-gravitational accelerations to achieve acceptable navigation accuracies; this technique has been proven in flight on Discovery-class missions such as Near Earth Asteroid Rendezvous (NEAR) Shoemaker and Stardust.

To account for the effects of solar radiation during cruise and during Mercury orbit, a numerical "box" model of the spacecraft, consisting of approximately 30 flat plates, is being developed. For the orbit phase, this modeling will also incorporate radiation from Mercury, expected to be the largest single force (after Mercury's gravity) to perturb the spacecraft orbit. This procedure has been utilized successfully on the Mars Global Surveyor (MGS) and NEAR Shoemaker missions.

## 3. Spacecraft

### 3.1. System overview

A ballistic Mercury mission on a Delta launch vehicle is challenging from mass, thermal, and fault-protection perspectives. These challenges are met for MESSENGER with a combination of carefully selected advanced technologies and a design philosophy that values simple, proven techniques. Mass is reduced through an integrated design for the composite structure and a high-performance propulsion system. The very challenging thermal environment at Mercury is addressed through innovative use of materials and by a carefully optimized mission geometry. Reliability

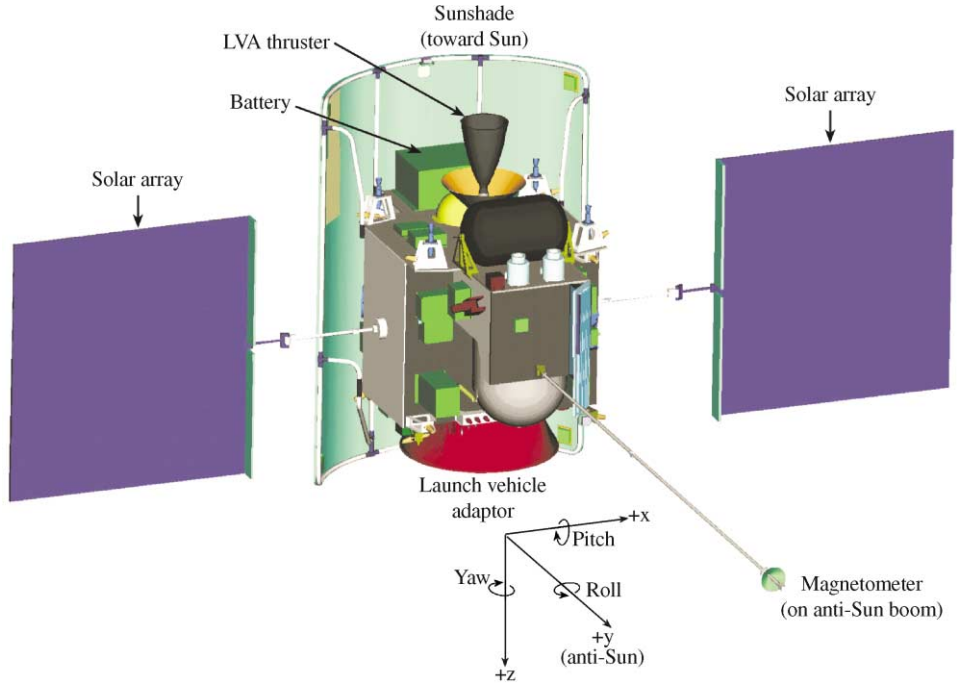


Fig. 3. The MESSENGER spacecraft is shown in the deployed configuration. The sunshade protects the spacecraft from the direct solar illumination to the extent that it allows the use of standard space-grade electronics. The only other major element exposed to the Sun is the solar array, which is composed of 30% cells and 70% mirrors. The large area of mirrors reduces the panel operating temperatures to that experienced in Earth-orbiting concentrator solar arrays. Both of these elements are designed to have excess margin during the orbital phase, reducing the sensitivity of the designs to the unknowns of the Mercury environment.

Table 4
Master equipment list

| Equipment list | Qty | Redundancy | Mass (kg) | Cruise power (W) | Orbit power (W) |
|---|---|---|---|---|---|
| Imagers (MDIS) | 1 | Functional | 5.5 | 0.0 | 10.0 |
| Gamma-Ray Neutron Spectrometer (GRNS) | 1 | Functional | 9.0 | 0.0 | 4.5 |
| X-Ray Spectrometer (XRS) | 1 | Functional | 4.0 | 0.0 | 8.0 |
| Magnetometer with boom (MAG) | 1 | None | 3.5 | 0.0 | 2.0 |
| Mercury Laser Altimeter (MLA) | 1 | None | 5.0 | 0.0 | 20.0 |
| Mercury Atmospheric and Surface Composition Spectrometer (MASCS) | 1 | Functional | 2.5 | 0.0 | 3.0 |
| Energetic Particle and Plasma Spectrometer (EPPS) | 1 | None | 2.25 | 0.0 | 2.0 |
| Data Processing Unit (DPU) and instrument power | 2 | Full | 5.0 | 0.0 | 18.0 |
| Instrument harness, brackets, and attachments | 2 | None | 3.25 | | |
| Instrument subtotal | | | 40.0 | 0.0 | 67.5 |
| Oxidizer tank | 1 | None | 8.0 | | |
| Main fuel tanks | 2 | None | 16.0 | | |
| Helium tank | 1 | None | 10.0 | | |
| Auxiliary fuel tank | 1 | None | 2.5 | | |
| 645-N bipropellant thruster | 1 | None | 4.0 | | |
| Monopropellant thrusters | 14 | Selective | 4.7 | | |
| Regulators, valves, filters, lines, and misc. | --- | Selective | 26.2 | 8.0 | 8.0 |
| Propulsion subtotal | | | 71.4 | 8.0 | 8.0 |
| Solar panels | 2 | Functional | 24.2 | | |
| Solar array drives and deployment system | 2 | Full | 10.5 | 0.0 | 1.0 |
| Power system electronics | 2 | Full | 18.7 | 23.0 | 23.0 |
| Battery | 1 | Functional | 21.0 | 8.0 | 0.0 |
| Power subtotal | | | 74.4 | 31.0 | 24.0 |
| Phased-array antenna assemblies | 2 | Functional | 3.3 | | |
| Low-gain and medium-gain antenna assemblies | 2 | Functional | 2.4 | | |
| Transponders | 2 | Full | 6.2 | 24.6 | 24.6 |
| RF power amplifiers | 2 | Functional | 5.6 | 52.0 | 52.0 |
| Diplexer, switches, waveguide, and coaxial cable | --- | Full | 5.3 | | |
| Telecommunication subtotal | | | 22.8 | 76.6 | 76.6 |
| Reaction wheels | 4 | 4 for 3 | 13.0 | 15.0 | 15.0 |
| Star cameras | 2 | Full | 5.3 | 8.0 | 8.0 |
| Inertial measurement unit with accelerometers | 1 | Full | 5.6 | 23.0 | 23.0 |
| Digital sun sensors and electronics | 2 | Full | 3.1 | 2.0 | 2.0 |
| Guidance and control subtotal | | | 27.0 | 48.0 | 48.0 |
| Integrated electronics module (IEM) | 2 | Full | 10.8 | 31.4 | 40.3 |
| Remote interface unit | 1 | Full | 2.1 | 4.0 | 4.0 |
| IEM subtotal | | | 12.9 | 35.4 | 44.3 |
| Thermal subtotal (sunshade, blankets, heaters) | --- | Full | 28.4 | 105.0 | 70.0 |
| Structure subtotal | --- | None | 71.2 | | |
| Harness | --- | Selective | 31.8 | 4.5 | 4.9 |
| Dry mass and power totals | | | 379.9 | 308.5 | 343.3 |
| System mass and power capabilities | | | 476.2 | 370.0 | 450.0 |
| Required propellant and helium | | | 607.8 | | |
| Backup mission holdback | | | 9.0 | | |
| Dry mass and power margins | | | 25.3% | 20.0% | 31.1% |

is heightened by using maximum heritage from other missions and simplifying the hardware and software wherever possible. This approach produces a design with ample margins in all categories and low technical and cost risk.

A view of the spacecraft in flight configuration is shown in Fig. 3. System-level margins for mass and power and system redundancies are given in Table 4. Key requirements and margins are listed in Table 5.

MESSENGER is a 3-axis, zero-biased, momentum-controlled spacecraft. It has only a single pointing mode during cruise: the sunshade is pointed at the Sun, and the rotation axis of the solar panels is aligned in the ecliptic plane. The direction of the bipropellant thruster (large velocity adjust, LVA) is oriented normal to the spacecraft-Sun line to accommodate maneuvers in this attitude. Communication is maintained at all times in this fixed attitude by

Table 5
Requirements, performance, and margins

| System | Requirement | Calculated performance | Margin |
|---|---|---|---|
| Mass | 476.2 kg maximum dry mass | 379.9 kg | 25.3% margin |
| Propellant | 2190 m/s | 2300 m/s | 110 m/s |
| *Power* | | | |
| solar array, cruise | 308 W cruise phase | 370 W cruise phase | 20% margin |
| solar array, orbit | 343 W orbit phase | 450 W orbit phase | 31% margin |
| battery | $<$ 60% max discharge | $<$ 46% worst chase | 23% |
| *Attitude system* | | | |
| control | $0.1^\circ$ ($1\sigma$) pointing and control | 500 μrad ($1\sigma$) | Factor of 2.5 |
| knowledge | 350 μrad ($1\sigma$) | 250 μrad ($1\sigma$) | 40% |
| maneuver | $0.005^\circ/s^2$ acceleration, $0.1^\circ$/s slew rate | $0.006^\circ/s^2$, $0.3^\circ$/s | 20% acceleration, factor of 3 slew |
| jitter | 25 μrad in 0.1 s ($1\sigma$) | 15 μrad in 0.1 s ($1\sigma$) | 66% |
| *Thermal (orbit avg.)* | | | |
| electronics | $-29$ to $60^\circ$C operational, $< 5^\circ$C/min | $-10$ to $30^\circ$C, $< 2^\circ$C/min | $19^\circ$C cold, $30^\circ$C hot, $3^\circ$C/min |
| instruments | $-20$ to $25^\circ$C for in-cal, $< 5^\circ$C/min | $-14$ to $8^\circ$C, $< 2^\circ$C/min | In calibration 99.5% of time at Mercury |
| solar arrays | $135^\circ$C operational, $180^\circ$C survival | $180^\circ$C operational, $250^\circ$C survival | $45^\circ$C operational, $70^\circ$C survival |
| battery | $-10$ to $25^\circ$C | $-5$ to $19^\circ$C | $5^\circ$C cold, $6^\circ$C hot |
| Telemetry downlink | 5.5 Mbytes/day, orbit phase | 9.8 Mbytes/day, orbit phase | 78% (with 1.5 dB link margin) |
| Recorders | 4.22 Gbits | Two redundant 8-Gbit SSRs | Factor of 2.5 |
| Flight software (main processor) | 20 MHz, 32 bit CPU, 8 Mb memory | $<$ 45% of CPU and memory | Factor of 2 |
| 1553 data bus | 194 kHz with 100% retransmit overhead | 1.0 MHz | Factor of 5 |
| Radiation tolerance | 30 krad total dose behind 2 mm aluminum | Worst-case 13-krad total dose | Factor of 1.3 |

medium-gain and high-gain antenna clusters on the forward and aft sides of the spacecraft. During on-orbit operations, rotation about the Sun line is required to accommodate instrument viewing, since the instrument-view direction is normal to the spacecraft–Sun line and opposite the LVA direction. Although thermal requirements are always met, high-rate downlink communications are not maintained during the rotation periods. During the data downlink periods, generally scheduled when the spacecraft is away from periapsis, the spacecraft roll axis is controlled so that one of the high-gain antennas can acquire Earth.

The system block diagram, detailing all the subsystem interfaces, is shown in Fig. 4. The subsystem interfaces are designed to limit the amount of time-sensitive, high-speed, or noise-sensitive data flowing across subsystem boundaries. In particular, the spacecraft interfaces only to the instrument Data Processing Unit (DPU) for access to the entire instrument suite. This method of clean-interface partitioning allows parallel subsystem development and minimizes the probability that a design change impacts more than a single subsystem. The majority of subsystem interfaces are over an MIL-STD 1553 serial data bus, compatible with many off-the-shelf, standard industry components.

Other highlights of the design include the following:

*Structure/Propulsion*. A composite structure using the snap-together construction technique (Snapsat®) pioneered by Composite Optics, Inc. (COI), is integrated with an Aerojet-supplied dual-mode propulsion system to achieve a lightweight spacecraft. The efficient, dual-mode propulsion system minimizes the number of tanks and associated plumbing, while maintaining a high average specific impulse ($I_{sp}$).

*Thermal*. A passive thermal design, based on innovative use of conventional materials, enables the use of standard space-grade electronic parts. Maintaining a fixed, opaque ceramic-cloth sunshade between the spacecraft and the Sun creates a benign thermal environment for the spacecraft. The shade requires no deployment. It allows the spacecraft to be tilted normal to the Sun line by $\pm 15^\circ$ in yaw and $\pm 12.7^\circ$ in pitch without exposing the spacecraft body to direct solar illumination. The thermal design also protects the spacecraft when it is near the hot Mercury surface.

Solar panels project beyond the sunshade and are rotatable. On-board software controls the solar aspect to balance panel temperature and power generation. The front faces of the panels are populated with 70% optical solar reflectors (OSRs) and 30% GaAs/Ge cells; the back faces are covered by Kapton with a vapor-deposited aluminum outer layer. This design reduces the peak expected temperature by $150^\circ$C over that of a fully-packed array under full Sun at 0.3 AU (Fig. 5).

Prototype MESSENGER solar panels have recently been thermal cycled at JHU/APL and illuminated at intensities appropriate for Mercury ($>$ 10 Suns equivalent) using

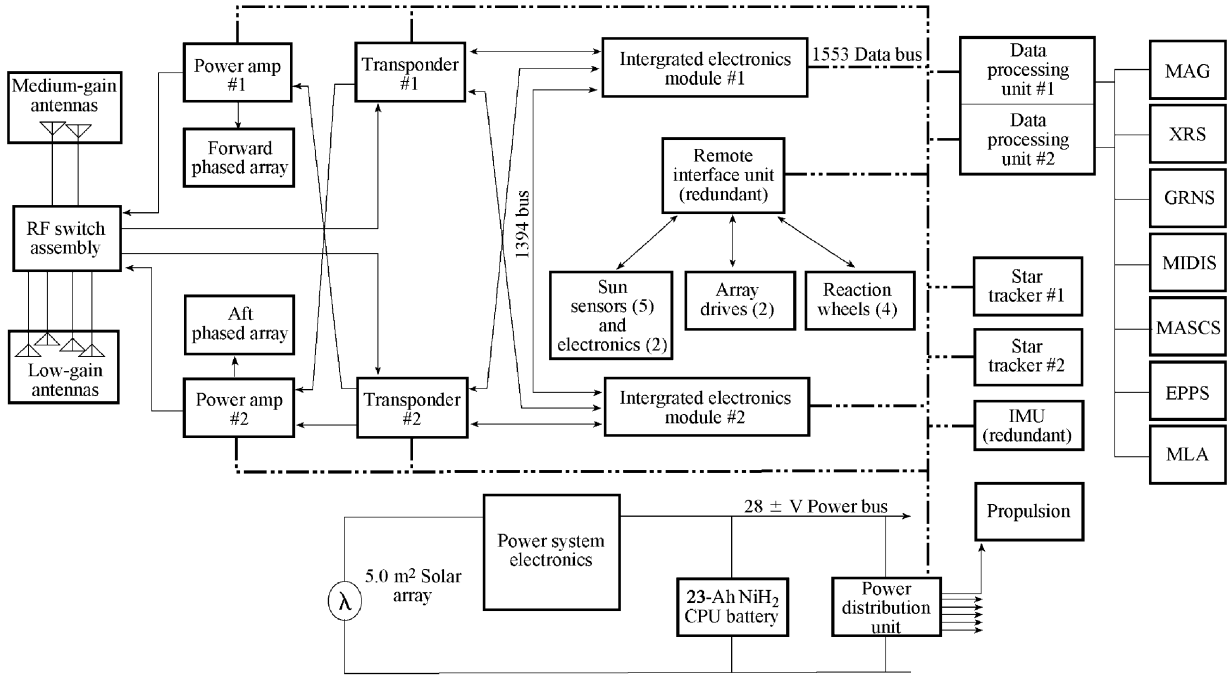


Fig. 4. The spacecraft block diagram illustrates the high degree of redundancy and cross-strapping of the hardware elements. The architecture uses off-the-shelf commercial components where available. Extensive use is made of the highly fault-tolerant 1553 data bus to interface systems. During integration and test, the actions of the flight guidance and control sensors and actuators can be simulated over a test port of the 1553 data bus. This capability allows the spacecraft flight software to be fully tested on the flight vehicle using a ground-based dynamic attitude simulator.

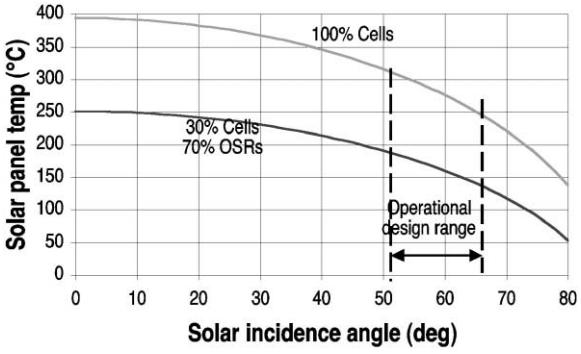


Fig. 5. The use of 70% optical solar reflectors reduces panel temperatures substantially from an array fully packed with cells. A major benefit of adding the reflectors is the lower required survival temperature in the event that the front or back of the array is pointed directly at the Sun as a result of an attitude anomaly. The MESSENGER array is designed to survive any pointing anomaly at any time during the mission without damage.

solar simulators under vacuum at NASA's John H. Glenn Research Center at Lewis Field (GRC). These tests validated many parts of the thermal model that depend on the optical properties of the panel, characterized the thermal conduction properties of the panel, and demonstrated panel survivability at the worst-case, normal-incidence conditions. No failures were experienced.

*Power*. The power system uses a fault-tolerant, peak-power-tracking architecture, allowing a small solar array to handle the wide temperature range experienced between 0.3 and 1.0 AU. This system is employed on the JHU/APL Thermosphere, Ionosphere, Mesosphere Energetics and Dynamics (TIMED) spacecraft. The battery uses available common-pressure-vessel technology, with 11 vessels and two cells per vessel. It is designed to function with the failure of one vessel. The power system maintains in excess of 20% power margin over the entire mission with a maximum battery discharge of 46%.

*Communications*. An X-band coherent communications system incorporates redundant Motorola small deep-space transponders, two lightweight phased arrays for downlink, and medium-gain and low-gain antennas for uplink and downlink communications. The antennas are chosen to enable high-rate and safe-mode communications over the entire mission while maintaining the sunshade pointing at the Sun. The electronically steerable phased arrays are used instead of a deployed, gimbaled high-gain antenna to increase reliability by reducing critical non-redundant moving parts. They are simple, passive waveguide antennas fed by solid-state power amplifiers (SSPAs) that are safely located inside the spacecraft body.

*Electronics*. Redundant integrated electronics modules (IEMs) incorporate all of the spacecraft avionics and software, including command and data handling and attitude processing. This approach, combining all of the digital spacecraft processing into a single unit, reduces box and harness mass. Each of the redundant IEMs contains two 32-bit

processors. The central processing unit (CPU) and memory requirements within both computers are budgeted at $< 45\%$ of the machine resources. Communications between the redundant IEMs are carried over a high-speed, fault-tolerant, redundant IEEE-1394 serial bus. The instrument timing, commands, and low-rate telemetry collection are over a redundant, fault-tolerant MIL-STD 1553 serial data bus. The 1553 bus has the following attractive features: a reduction of interconnecting cables, built-in redundancy and cross-strapping, a highly fault-tolerant transformer-coupled interface, a common-data architecture for sharing information between subsystems, and a flexible software-defined interface. Both the IEEE-1394 and MIL-STD 1553 interfaces are budgeted at $< 20\%$ of the available bandwidth.

*Command and data handling*. The command and data-handling system implements Consultative Committee for Space Data Systems (CCSDS)-compliant uplink and downlink protocols. Command memory is sized to allow on-orbit storage of two weeks of orbital-phase operations. Data handling supports simultaneous telemetry collection from all of the instruments at their maximum data bandwidth, eliminating the need for data-collection resource planning.

*Attitude control.* Attitude control is provided by a low-risk, reaction-wheel, attitude-control system, which is very similar to the hardware successfully used on the NEAR Shoemaker spacecraft (Santo et al., 1995). Pointing control of the solar panels and the phased-array antennas are computed with an on-board guidance algorithm, similar to the one implemented on NEAR Shoemaker (Santo et al., 1995). Fault-protection algorithms, implemented in redundant IEM computers and based on redundant solar detectors and temperature sensors, override any attitude maneuver that compromises the sunshade effectiveness or solar-array thermal limits.

### 3.2. Structure/propulsion system

The integrated structure/propulsion approach was developed jointly by team members GenCorp Aerojet, COI, and JHU/APL. The integrated structure shown in Fig. 6 utilizes two large vertical panels to support the two large fuel tanks. A third and fourth internal vertical panel support the heavier oxidizer tank and the plumbing panel. This design completes a rigid, yet very light, center column. The loads from this column flow directly into an aluminum adapter, compatible with the Delta II interface. This adapter is a flange, machined of 6061-T651 aluminum, which is bolted to the aft ends of the four vertical panels making up the center column.

Three composite panels, forming an open box, cover the top of each fuel tank, producing packaging area to mount spacecraft electronics. A three-piece composite-sandwich, bottom-deck panel adds stiffness and packaging area for the instruments, while a single top-deck panel mounts the LVA thruster, small thrusters, helium and auxiliary fuel tanks,

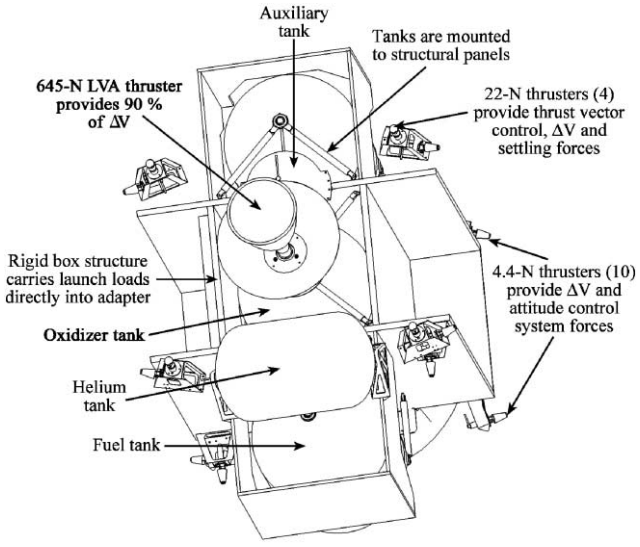


Fig. 6. The spacecraft structure is shown with the top deck and the side radiator panels removed. The structure design is extremely efficient, constituting less than 7% of the launch mass. Spacecraft components are mounted to the outside surfaces of the top deck, the bottom deck, and the open box structures covering the fuel tanks.

star trackers, and battery. This deck also acts as a radiator. Two side radiator panels complete the box structure and add shear stiffness. The extremely short, direct load paths in this stiff-box arrangement result in a low primary-structure mass. The compact structure (1.27 m wide $\times$ 0.71 m deep $\times$ 1.05 m tall) provides sufficient panel and deck area for all instruments and electrical components.

The sunshade is supported by a welded 3Al–2.5V titanium-tube assembly. The assembly supports four Sun sensors, a solar-flux monitor (for the X-Ray Spectrometer, see Gold et al., 2001), the forward phased-array, and the medium-gain and low-gain antennas.

Deployment mechanisms are limited to the solar array and the magnetometer. During launch, the solar arrays are supported using a ball-and-socket center hold down and four 'V'-flexure joints per wing. A pyrotechnic-release mechanism preloads each panel against the fittings. The 3.6-m magnetometer boom is of a two-piece, two-hinge design. The pyrotechnic, cable-cutter-release mechanism preloads the boom against the spacecraft prior to deployment.

The structure/propulsion unit is being collaboratively fabricated and integrated by team members Aerojet and COI, under subcontracts to JHU/APL. The unit's stiff, lightweight properties result from a deliberate effort to optimize launch load paths. All of the large tanks are supported by brackets mounted to the vertical panels. Under thrust, tank loads and deck loads are reacted into the vertical panels and carried directly into the adapter. With the exception of the aluminum adapter, the structure is made of graphite-cyanate-ester (GrCE) composite. JHU/APL has flown this material in the NEAR Shoemaker high-gain antenna (Bokulic et al., 1998), and COI has extensive

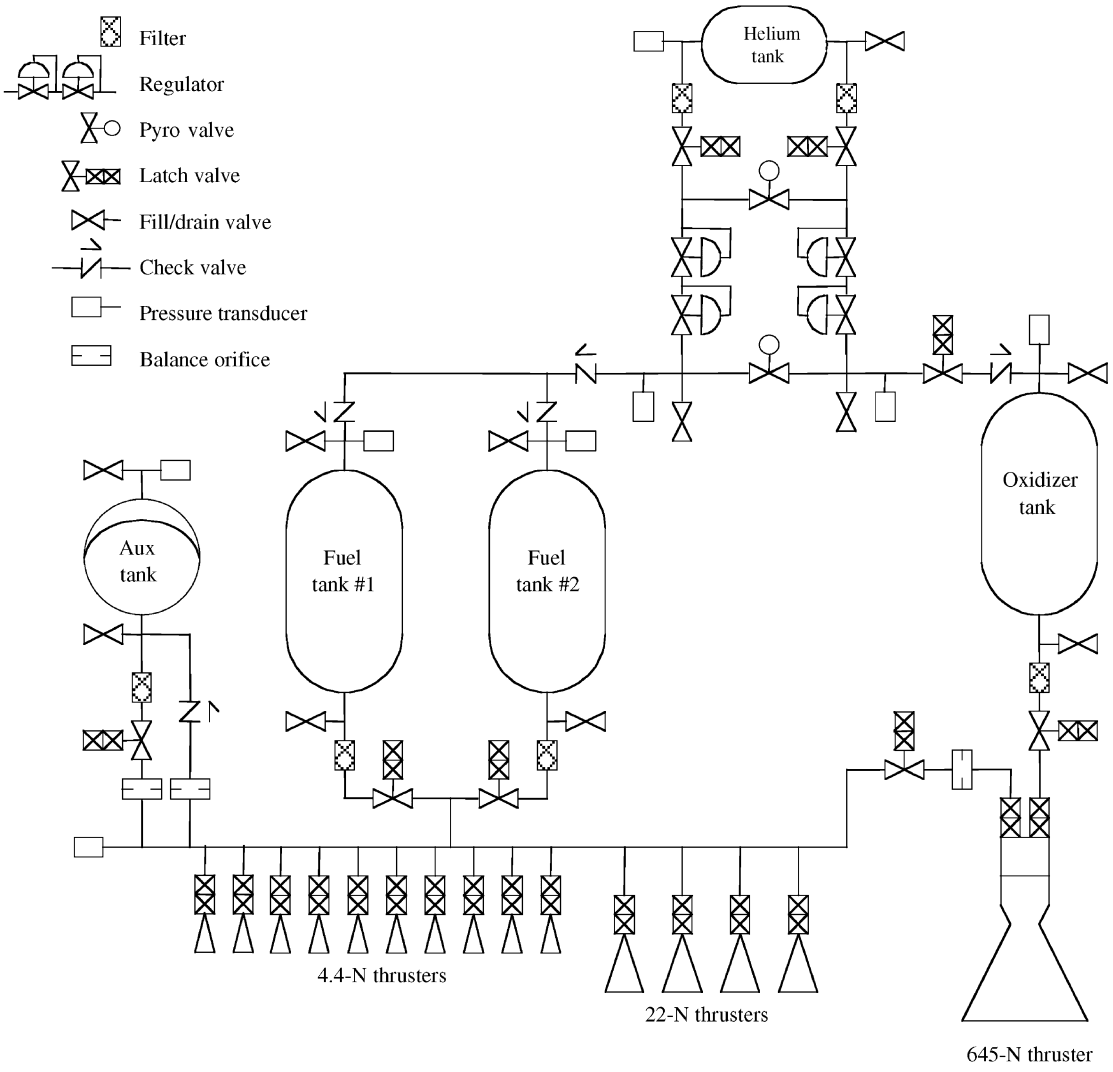


Fig. 7. The dual-mode propulsion system is very mass efficient. A custom titanium tank design, common for both the oxidizer- and fuel-tank designs, is central to meeting the low-mass target. The MESSENGER propulsion system carries twice the propellant of the NEAR Shoemaker system with less mass. Dual feeds from the helium tank preclude oxidizer mitigation problems. Pyrotechnic-activated latch valves, located upstream and downstream of the regulators, enhance system reliability.

experience with this material in many lightweight, low-cost spacecraft structural sandwich applications.

The structure readily lends itself to COI's Snapsat® technique of using flat stock to create isogrid and orthogrid panels, composed of opposing face skins with discrete internal ribs. The face skins are relieved in areas where structure is not required, leaving an 'I' flange cross section. Rib design and spacing are customized to react to specific loads. Egg-crating and mortis-tenon joining techniques are used to assemble flat stock to the panels and the panels into the box structure. This approach minimizes cost by eliminating molded details. It is self-tooling and uses computer-aided manufacturing software to verify the design and turn it into manufacturing databases. The composite design uses Fiberite M55/954-3 GrCE material in a pseudoisotropic lay-up. All mated surfaces in the structure are bonded using the high-strength space-qualified adhesive Hysol EA9394.

The propulsion system, designed and fabricated by GenCorp Aerojet, is mounted directly to the structure. The propulsion system schematic is shown in Fig. 7. The main LVA thruster is a 645-N, 317-s $I_{sp}$ Leros-1b bipropellant unit developed for the A2100 satellite family. Four 22-N, monopropellant thrusters provide steering forces during main thruster burns and primary propulsion for most of the smaller $\Delta V$ maneuvers. Ten 4-N, monopropellant thrusters are arranged in two double-canted sets of four for attitude control, plus two for providing velocity in the sunward direction. They provide redundant three-axis attitude control, pure-couple, momentum-dumping torques, propellant-settling forces, and fine-$\Delta V$ control in all three axes. A state-of-the-art, regulated dual-mode system,

the propulsion system has been designed to provide the mission-required 2300 m/s using the highest-performance, lightest-weight components and technology presently available.

The performance is optimized by allocating over 90% of the propellants for bipropellant use and by minimizing the tank mass. Tank mass and cost are minimized through an innovative application of a very small auxiliary fuel tank. Adding this small fuel tank enables the large fuel and oxidizer tanks to become much lighter and less expensive by allowing in-line trap propellant management devices and vortex baffles in place of diaphragms. Small, 2-m/s monopropellant settling burns use the auxiliary fuel tank, which has an elastomeric diaphragm, in blowdown mode prior to each bipropellant burn to settle the propellant at the tank outlets. The auxiliary fuel tank supports up to 65 m/s of maneuvers before refilling. It is refilled during the bipropellant firings through operation of the auxiliary tank latch valve. The propulsion system has sufficient capacity to hold the required propellant at its maximum temperature (40°C) over the specified range of main engine mixture ratio (0.85–0.90) with a 5% volume margin to allow extra propellant to be loaded if the dry spacecraft mass is below maximum at launch.

Propulsion system redundancy is derived from that used on NEAR Shoemaker (Mosher and Wiley, 1998). Dual high-pressure regulators that independently feed the fuel and oxidizer sides are series redundant and leakage protected by the high-pressure latch valves. Pyro valves are inserted upstream and downstream of the regulators to protect against failure in either a high-pressure latch valve or a regulator. Check valves are internally parallel-redundant at the component level and series-redundant on the fuel side. The propellant latch valves have redundant coils. The monopropellant thrusters have series-redundant valves, redundant coils, and redundant cat-bed heaters. The monopropellant thrusters provide redundant 3-axis attitude control. By design, there are no potential single-point failures throughout the wiring, connections, heaters, and thermostats. The list of single-string items includes all five tanks, all propellant latch valves, the oxidizer inlet latch valve, all latch valve position indicators, the propellant filters, and the bipropellant thruster.

The system is pressurized from a 38.6-MPa, 5000-pounds-per-square-inch-absolute (PSIA) Maximum Expected Operating Pressure (MEOP) dual-outlet helium tank feeding two series-redundant regulators through filters and high-pressure latch valves. The Pressure Systems, Inc. (PSI), 80374 titanium-lined, graphite-composite overwrapped helium tank, qualified for A2100, satisfies all helium tank requirements. Regulated pressure at 1.85 MPa (240 PSIA) feeds the propellant tanks through redundant check valves and, on the oxidizer side, an additional isolating latch valve. The pressurization system design and heated pressurization manifold preclude any Mars-Observer-type vapor migration problems.

Three identical main propellant tanks, two fuel and one oxidizer, feed the thruster complement through filters, activation-surge-limiting venturis, and flow-sequencing latch valves. The currently baselined titanium propellant tank will be designed per MIL-STD-1522A to an MEOP of 1.93 MPa (250 PSIA) gauge pressure and a burst/MEOP factor of safety of 1.5. During all ground test and launch operations, tank pressure will be limited to 1.38 MPa (180 PSIA) to provide a $> 2.0$ factor of safety. By using identical tanks, the tank qualification, tooling, and manufacturing costs are minimized. By selecting an all-titanium approach, the development risks and range safety issues associated with overwrapped propellant tanks are eliminated.

A small auxiliary diaphragm fuel tank uses PSI's 80290 titanium AF-E-332 diaphragm tank qualified for the Interim Transfer Vehicle (ITV) to provide the required 12.4-l capacity. All bipropellant burns are preceded by a settling burn sequence using the auxiliary fuel tank and two 22-N monopropellant thrusters.

### 3.3. Thermal design

The thermal design is completely passive, requires no louvers or other mechanisms, uses readily available materials, and needs little heater power. This elegant design is enabled by the mission geometry. During the orbital phase, the distance between the Sun and Mercury varies from 0.30 to 0.47 AU, corresponding to a solar flux variance from 11.1 to 4.5 times that received at Earth. This flux is unidirectional and is effectively attenuated by the sunshade. A second source of thermal input to the spacecraft is the infrared (IR) energy emitted by the sunlit side of Mercury. The maximum surface temperature of Mercury reaches 433°C at its perihelion and falls off to 298°C at its aphelion. The temperature drops off as a cosine function from the maximum at the subsolar point to −173°C at the dawn terminator (Wertz, 1978). The IR heat flux is omnidirectional and cannot be effectively attenuated. The spacecraft orbit is carefully chosen to minimize the IR radiation received from Mercury's surface. The orbit is highly elliptical and the periapsis latitude is at 60°N, well away from the subsolar point, but where the orbital velocity at the subsolar crossing point is still very fast. Further, the spacecraft crosses the subsolar point close to the planet at true anomaly (TA) 237° or 0.41 AU, well away from perihelion (Fig. 8).

Throughout the mission, the sunshade is pointed at the Sun and the spacecraft is rotated about the Sun line to accommodate instrument viewing. The general approach for thermal management is to reduce the heat load on the Sun side of the spacecraft via the sunshade to the point where radiating panels on three sides of the structure can remove any excess heat. As the spacecraft passes over the hot side of the planet, IR energy is absorbed into the spacecraft body through the side radiator panels, causing a brief temperature spike. When the spacecraft moves away from the planet

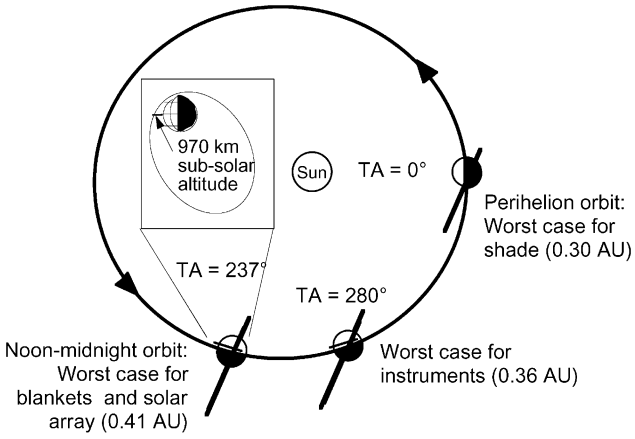


Fig. 8. A detailed thermal model was created to predict the worst-case environment for different spacecraft components. This model was necessary since the worst-case design points are not intuitive. A design without this model would require that all of the worst-case environment assumptions be made simultaneously, and would drastically increase the mass required to satisfy the thermal requirements.

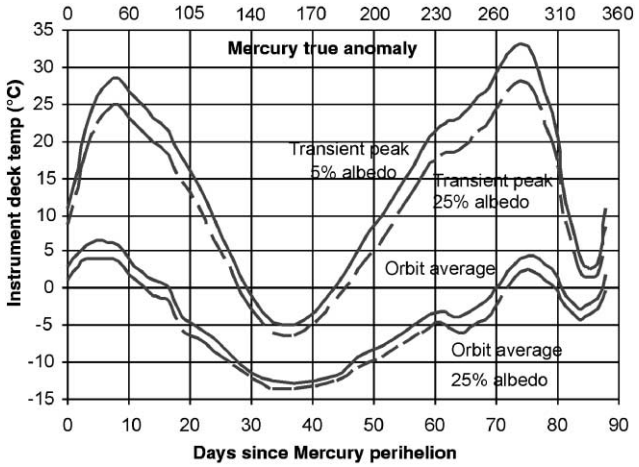


Fig. 9. The average and peak instrument deck temperatures are shown over a Mercury year for two very different assumptions regarding average planetary albedo. Throughout the majority of the 12-h orbital period the heat given off by the planet does not affect the spacecraft. Therefore the average deck temperature is largely a function of the solar distance. At true anomaly $0^{\circ}$ the distance is a minimum and at true anomaly $180^{\circ}$ the distance is a maximum. The transient temperatures are reached during the short portion of the orbit when the spacecraft is in the vicinity of the sunlit side of the planet. The transient temperatures, therefore, are a function of both how much time the spacecraft encounters the sunlit side of the planet and the solar distance.

this excess heat is radiated and the spacecraft returns to its steady-state temperature. The radiators have sufficient total area to handle the worst-case heat load. They are isolated from the spacecraft structure and spacecraft electronics, coupled only through radiation, dampening the effect of the IR heat flux received during the 25-min planet crossings. The solar arrays have IR shields installed on the sides of the panels closest to the spacecraft and are placed on low-conductive struts, 0.9 m from the side radiator panels, to reduce heat coupling to the spacecraft. A thermal analysis to determine the minimum survivability duration for an unplanned attitude anomaly, where solar illumination directly heats the back side of the spacecraft, is underway.

The spacecraft is designed to run near its cold-operating limit during cruise phase, when the spacecraft is in a low-power mode, so that when all instruments are powered during orbital operations the spacecraft remains below its upper operating-temperature limit. There are no thermal concerns during the Venus or Mercury flybys, as the closest approaches are all over shadowed portions of the planets. Thermal multilayer insulation with a Nextel outer layer covers the entire spacecraft, except for the radiator surfaces, which are covered with OSRs, and instrument apertures. The propulsion system, sunshade, battery, solar array struts, and some instruments are thermally isolated from the spacecraft using multilayer insulation and low-conductivity mounting hardware. The large bipropellant thruster is surrounded by a gold-plated heat shield to protect the spacecraft during burns. All spacecraft heaters are redundant and are controlled by mechanical thermostats. The set-points of the primary and secondary heaters are offset so that the secondary heaters are never energized unless a primary heater fails.

The worst thermal case for the instruments occurs when the spacecraft periapsis is near the subsolar point (Figs. 8 and 9, day 75) at a distance of 0.36 AU from the Sun. The maximum temperatures are due to the IR and visible radiation from the planet; temperatures were computed for both 5% and 25% bond albedos for the planet, bracketing the uncertainty (Ercol et al., 2000). The worst-case hot instrument-deck orbit-average temperature is $7^{\circ}$C, and the worst transient is $33^{\circ}$C. The temperature transient profile for this orbit lasts only 25 min, with a maximum temperature gradient of $1.5^{\circ}$C per minute. During the remainder of the 12-h orbit, the temperature is near the orbit-average value. The payload is thus kept within its calibration temperature range over $\geqslant 99.5\%$ of the orbit phase and provides survival margins in excess of $20^{\circ}$C. Similar calculations verify that the spacecraft electronics are always within their $-29^{\circ}$C to $+60^{\circ}$C operating range with less than a $5^{\circ}$C-per-minute gradient. The battery always remains within its $-10$ to $+25^{\circ}$C operating range. For the majority of the mission, the battery temperature is maintained by heaters to be between $-5$ and $0^{\circ}$C. During the eclipse cycles, the battery temperature does peak to $19^{\circ}$C, but lifetime concerns are mitigated because only 200 discharge cycles are anticipated.

The sunshade is constructed from 3M Nextel 312 ceramic cloth covering both sides of a conventional all-Kapton multilayer blanket core (Fig. 10). The ceramic cloth is rated in excess of $1000^{\circ}$C. Under worst-case conditions, a $400^{\circ}$C temperature difference will exist between the sunshade and the spacecraft (Ercol et al., 2000).

A sample thermal Nextel shade and sunshade blanket were fabricated and tested under solar simulation in vacuum at NASA's GRC. The shade was not cleaned, and $30^{\circ}$C

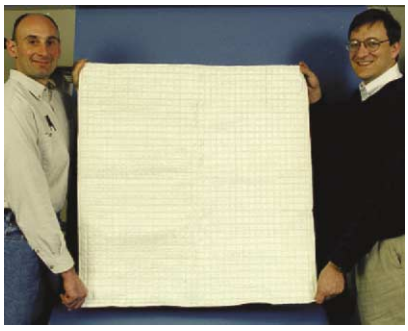

Fig. 10. A sample sunshade was fabricated and tested at a solar intensity of 11 Suns, representing the environment at 0.3 AU (Fig. 11). The sunshade eliminates direct solar heating and provides a room-temperature environment for the spacecraft.

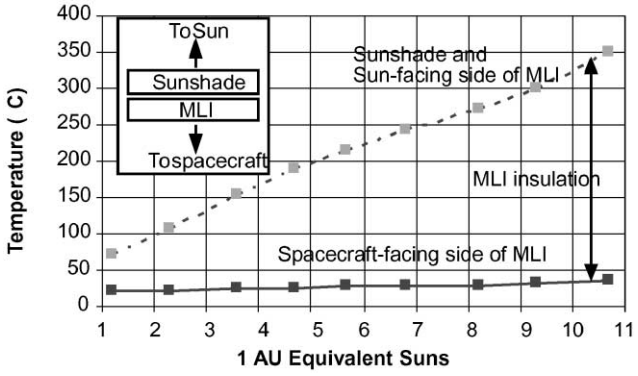


Fig. 11. Test results at GRC show the insulating capability of the sunshade. The temperature of the spacecraft-facing side of the shade is flat over the varying solar distances. From this result it can be deduced that the shade's insulting properties are very insensitive to the shade's optical surface qualities; if the shade surface degrades (effectively increasing the temperature of the Sun-facing surface) the temperature of the back side of the shade remains unchanged.

chamber walls were used, which bias the results on the hot side. At 10.7 times the solar flux received at Earth, the shade surface measured 350°C, the Sun-facing side of the multilayer insulation (MLI) behind the shade measured 350°C, and the spacecraft-facing side of the MLI measured 35°C (Fig. 11) (Mason, 1999). These tests demonstrated the ability of the sunshade configuration to ameliorate high temperatures and validated the expected performance of the MLI. Results from the thermal model, with the shade thermal properties degraded at the worst-case end-of-life conditions, indicate that the orbit-average spacecraft temperature is between 5 and 25°C.

The solar monitor, four Sun sensors, a medium-gain antenna, three low-gain antennas, and the forward phased array look through the sunshade. All are located at the ends of the shade to give a clear view to space for backside heat radiation. The sunward-facing sides have opaque, white ceramic matrix composite (CMC) covers or attenuating filters as appropriate to reduce detector heating. For the antennas, the CMC cover acts as a radome at the same temperature as the sunshade. The faces of the antennas that view the radomes are coated with a low-emissivity material (such as gold or vacuum-deposited aluminum) to reduce IR irradiance from the radome by at least an order of magnitude.

### 3.4. Telecommunications system

The X-band telecommunications system is designed to provide the required science return, a reliable spacecraft command link, and precise radiometric tracking data. It incorporates redundant X-band transponders to provide command, telemetry, and high-precision Doppler/ranging capability (Fig. 4). Power amplification is provided by SSPAs. The system is cross-strapped on both sides of the transponders, providing near-full redundancy on both the uplink and downlink. The only components not cross-strapped are the distributed power amplifiers; each is dedicated to one phased-array antenna. The distributed nature of the phased array permits graceful degradation in the event of an amplifier-element failure. Even if a complete array were to fail, under worst-case conditions enough recorder capacity exists to store the orbit-phase science data and downlink those data later using the other array and a revised downlink schedule.

Antenna coverage is provided by two waveguide-based phased arrays (for the science downlink), two medium-gain fanbeam antennas (for commanding and low bit-rate downlinking), and four low-gain antennas (for burn mode, emergency, and near-Earth communications) (Fig. 12). Two identical 18 cm × 76 cm phased arrays, mounted on opposite sides of the spacecraft, eliminate the need for a gimbaled high-gain antenna (HGA). These arrays, constructed from established aluminum-waveguide technology, are rugged and low risk. The array design is kept simple by restricting the scanning capability to ±45° in one-dimension only. The design is further simplified by the use of transmit-only, linearly-polarized slot elements. The array is passive, with the electronics located in a power-amplifier assembly mounted within the spacecraft body. The antenna beamwidth is relatively large (12° × 3°), so effects due to thermal distortion are minimal. A full-scale brassboard model was built and tested with good performance (Fig. 13). Each phased array covers one full hemisphere by controlling the beam direction in one axis and rotating the spacecraft up to 360° about the spacecraft-Sun line. The medium-gain antennas (MGAs) each have a fanbeam pattern with a wideplane beamwidth of 90°. Medium-gain coverage, similar to the phased-array coverage, is obtained by rotating the spacecraft about the spacecraft-Sun line. Two low-gain antennas (LGAs) mounted forward and aft on the spacecraft, provide hemispherical coverage. Two additional LGAs, mounted on the top and bottom of the sunshade, provide communications during burns. The MGAs and LGAs all support both transmit and receive.

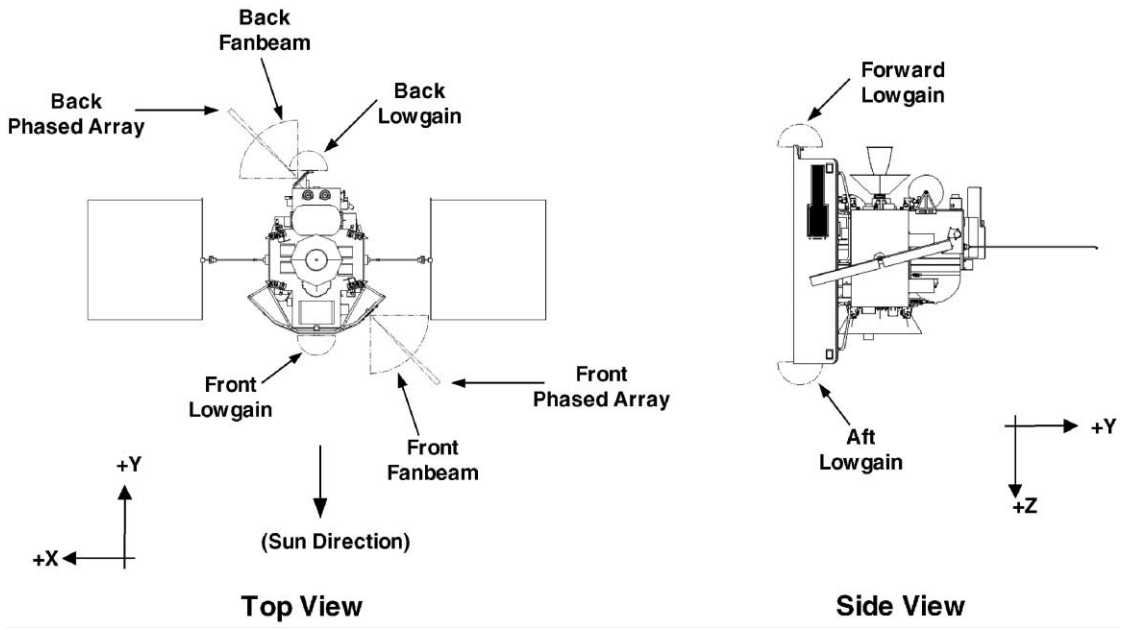


Fig. 12. The MESSENGER spacecraft antenna coverage is shown in two views. The phased-array and fanbeam antennas are co-located on each side of the spacecraft and provide coverage over one quadrant in the $X$–$Y$ plane. Coverage over an entire hemisphere is accomplished by rolling the spacecraft about the Sun-spacecraft line ($Y$-axis) so that the antenna pattern is aligned with the Earth direction. The front and back low-gain antennas are located along the $Y$-axis to provide maximum gain in that direction. The forward and aft low-gain antennas provide coverage during maneuvers.

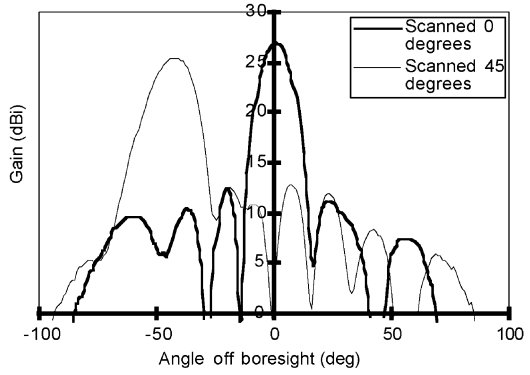


Fig. 13. Test results are shown from a brassboard phased-array antenna. These results show good gain and a scan loss at 45° that are very close to the theoretical value of −1.5 dB.

Motorola small deep space transponders (SDSTs) are at the center of the telecommunications system. Their design is well-established, having been first used on the New Millennium Deep Space-1 mission (Rayman and Lehman, 1997). The X-band signals from the transponders are amplified using SSPAs, for which JHU/APL has a rich heritage. Examples of recent JHU/APL experience include 5-W SSPAs built for the NEAR Shoemaker (Bokulic et al., 1998) and Midcourse Space Experiment (MSX) spacecraft and an 8-W X-band SSPA built for a military phased-array program. Two SSPA designs are required: a lumped SSPA providing 11 W to drive the MGAs and LGAs, and a distributed 11-W SSPA using eight 1.375-W amplifier modules (with phase shifters) to drive the phased array. During the majority of the cruise phase, the lumped amplifiers can be used to provide low bit-rate communications through the MGAs.

Table 6
Telemetry link budget for science return[a]

| Parameter | Value[b] | Notes |
|---|---|---|
| Transmitter power (dBm) | +40.4 | 11-W power amplifier |
| Spacecraft passive loss (dB) | −2.0 | Coax cables, radome |
| Transmit antenna gain (dBic) | +27.3 | Phased array, including scan loss |
| Path loss (dB) | −270.0 | Earth range = 0.6 AU; 8.43 GHz |
| Polarization mismatch loss (dB) | −3.0 | Linear-to-circular polarization |
| Other losses (dB) | −0.3 | Ground antenna weather, pointing losses |
| Receive antenna $G/T_s$ (dB/K) | +52.7 | DSN 34-m HEF antenna at 20° elevation, 90% weather |
| Phase modulation loss (dB) | −0.6 | Modulation index = 1.2 rad |
| Received $E_b/N_0$ (dB) | +3.5 | Bit rate = 9.0 kbps (using k = $1.38 \times 10^{-23}$ J/K) |
| Required $E_b/N_0$ (dB) | +1.0 | Rate 1/6, k = 15 convolutional coding + Reed Solomon |
| Receiver implementation loss (dB) | −1.0 | Block-V receiver system |
| Telemetry margin (dB) | +1.5 | |

[a]NOTE: $G/T_S$ = antenna gain per system noise temperature, $E_b/N_0$ = energy per bit-to-noise density ratio, dBm = decibels relative to 1 mW, dBic = gain relative to isotropic circular polarized antenna, DSN = Deep Space Network.

[b]Losses are expressed as negative numbers in decibels.

To predict orbital-phase data return, a link analysis (Table 6) was performed; a phased-array antenna for the

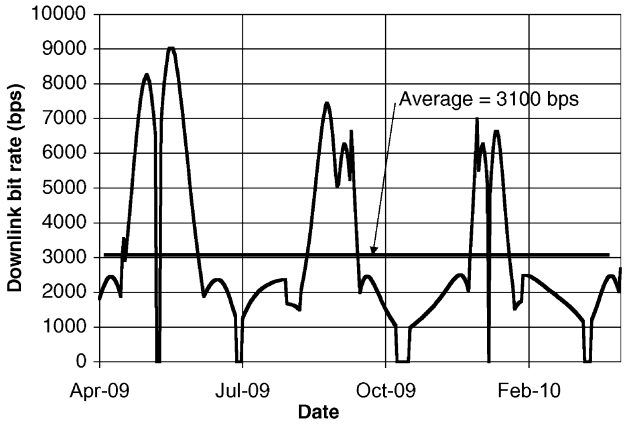


Fig. 14. The orbital-phase data return rate satisfies the mission requirements with a margin of 78%. The data downlink rate is a function of spacecraft-Earth distance. When the spacecraft passes within $2^{\circ}$ of the Sun, communication is prohibited. During these periods and when the spacecraft-to-Earth distance is great, the on-board recorder is used to buffer science data. During the periods of lesser spacecraft-to-Earth distances the recorder buffers are emptied.

downlink and the DSN 34-m ground antennas are assumed (Fig. 14). The analysis includes the varying spacecraft–Earth distance, solar effects, array scan-angle penalty, and linear-to-circular polarization loss. The average downlink bit rate (including data loss due to solar conjunction periods) is 9.8 Mbytes/day with a 1.5 dB margin, which satisfies the science requirement. An effort is underway to develop a circular polarization capability for the phased arrays, thereby increasing the downlink science return by up to a factor of two. The link analysis also shows that a Doppler precision of $< 0.1$ mm/s and a ranging precision of $< 10$ m are achievable during the Mercury orbit phase, satisfying the requirements of navigation and radio science.

### 3.5. Power system

The power system has a peak-power tracker (PPT) topology with strong heritage from the TIMED power system design. This architecture keeps any excess power at the array, eliminating the need for dissipative shunts within the spacecraft, while optimizing the solar array output over the highly varied operating conditions of the mission. The power system is composed of power-system electronics (PSE), a power distribution unit (PDU), a common-pressure vessel (CPV) 23-Ah $NiH_2$ battery, and a 5.0-$m^2$ solar array. The power subsystem design has no single-point failures. Within the PSE the battery-charge electronics and command and telemetry interfaces are fully redundant. The PPT electronics, also functionally redundant, consist of 8 pulse-width-modulated buck converters, or PPT modules, operating in parallel and sized so that any seven can fully support the mission. The PDU has fully redundant power-switching and distribution electronics. The battery is fault tolerant in that each of the cell vessels is bypassed by a contactor that is automatically activated to short the cell in case of an open-circuit failure of that vessel. The solar array is fault tolerant in that the solar cells are grouped into individual strings that are isolated with decoupling diodes. The calculated array power output assumes the loss of one string.

The spacecraft bus is tied directly to the battery, maintaining it at an unregulated 22–34 V. Within the PSE, the eight PPT modules are located in series between the solar array output and the spacecraft main power bus. The PPT modules control the power generated by the array by varying the operating voltage of the array. They set the array input voltage either at the maximum power point when the loads and battery recharge requirement can use the peak power of the array, or off the maximum point, toward the open-circuit voltage, when array power exceeds the loads. During peak-power operations, the array operating voltage is determined by an algorithm that is executed in an IEM processor. Hardware PPT backup controllers maintain a default array-voltage setting in the event of processor failure or restart.

Normally, the battery-charge control is performed by an IEM processor using coulometry and pressure-monitoring telemetry. Hardware algorithms based on voltage, temperature, and pressure prevent battery overcharge.

To execute power-switching control, the PDU receives commands from the MIL-STD 1553 serial bus. Commands are decoded, error-checked, and sent to a functionally redundant matrix arrangement of relays and power metal-oxide semiconductor field-effect transistor (MOSFET) drivers. The power-switching design has heritage in the TIMED design (Dakermanji et al., 1998), with improvements in mass efficiency by using power MOSFETs in place of larger relays. Fusing of power lines to each load is accomplished using replaceable, redundant fuse plugs attached to the PDU for easy fuse integrity verification throughout integration.

The solar array consists of two panels totaling 5.0 $m^2$ in area. The arrays are connected to drive motors whose rotation axis is normal to the Sun line to allow the panels to be rotated off solar normal. This maintains a nominal operational temperature of $135^{\circ}$C and insures operation below $180^{\circ}$C. A minimum margin of 20% is reached shortly after launch, when the spacecraft is at 1.0 AU. Greater margins exist during the inner-cruise and orbital phases as the Sun distance decreases. The array is constructed from materials that are each rated above $250^{\circ}$C. Cerium-oxide-doped borosilicate glass (CMX) is placed over the GaAs cells to mitigate radiation damage. The total charged particle radiation fluence, using 0.15-mm-thick CMX cover glass, is $2.0 \times 10^{14}$ equivalent 1-MeV electrons/$cm^2$ over the mission life.

The battery is a 23-Ah $NiH_2$ CPV design, similar to the one now flying on MGS. The CPV design offers significant mass and volume savings by combining two cells into each pressure vessel. The battery assembly consists of 11 vessels, each equipped with autonomous bypass circuitry in case of

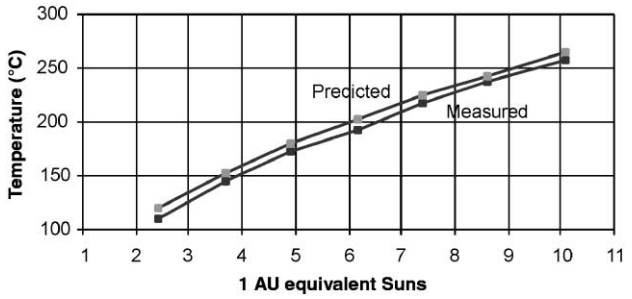


Fig. 15. Test results of a prototype MESSENGER solar array, pointed directly at the Sun, correlate well with the thermal model. The data points were taken at GRC as an increasing number of lamps were powered during the test. A critical part of the test was to measure the temperature gradient from the center of a cell to the cell's OSR interface. These data will be used to size the width of the flight cells for MESSENGER.

vessel failure. The bypass circuitry has heritage from Terra and TIMED (Dakermanji et al., 1998). The $NiH_2$ technology is well suited for MESSENGER by virtue of its low mass and tolerance to overcharge. The ability to measure battery pressure also provides an additional level of confidence in maintaining battery health. The maximum depth of discharge during the launch phase is 21%. The total number of battery discharge cycles during the cruise and orbital phases is approximately 200, with each cycle having a maximum depth of discharge less than 46% (51% with one vessel failed).

To demonstrate the survivability and robustness of the solar panel design and to validate thermal analyses, JHU/APL has successfully completed a series of high-temperature qualification tests including IR and solar simulator illumination heating of test articles. These tests were conducted on four test panels that were fabricated using standard manufacturing materials and processes. All panels were cycled in thermal vacuum from $-120^{\circ}$C to $+200^{\circ}$C and soaked at $250^{\circ}$C for 1 h without damage. One panel has also demonstrated no degradation during a 20-day extended soak at $180^{\circ}$C in rough vacuum and has shown no damage during a 30-min vacuum soak of $310^{\circ}$C. Another panel has also been illuminated in vacuum at the Tank 6 facility at NASA's GRC. The illumination flux was varied over a range of intensities with a maximum flux of 10.1 Suns, resulting in a maximum temperature of $257^{\circ}$C (Fig. 15) (Mason, 1999). During the test, the chamber walls were $30^{\circ}$C, which conservatively biased the test results toward higher temperatures. The test procedure contained several inspection points consisting of visual, electrical, and microscopic inspections to characterize panel survivability. The panels met all inspection criteria, demonstrating suitability for the MESSENGER mission. These results validated that the panel design can survive the worst-case failure mode of direct Sun pointing at 0.3 AU. In addition, the excellent correlation between the predicted and measured temperatures (Fig. 15) verified many of the optical-surface and conduction properties of the materials used in the thermal model, giving confidence in the design and the thermal model's accuracy.

### 3.6. Integrated electronics module

The spacecraft bus electronics are contained in redundant IEMs. Each function is implemented as a circuit card. Interfaces between cards inside an IEM are over a Peripheral Component Interconnect (PCI) backplane. A fault-tolerant and redundant IEEE-1394 serial bus interface is implemented between the IEMs to allow for card-level redundancy.

There are five cards in each IEM: (1) interface, (2) main processor (MP), (3) fault-protection processor (FPP), (4) solid-state recorder (SSR), and (5) power-converter. The interface card receives the CCSDS-compatible uplink bit stream from the transponders. It decodes and executes a subset of critical commands in hardware and passes the remaining commands to the MP card. The interface card also buffers and encodes CCSDS-compatible telemetry frames, sends the downlink bit stream to the transponders, houses the oscillator and timing chain electronics, and contains the high-rate serial link that facilitate 3.2-Mbps imager data transfer (Gold et al., 2001). The MP distributes all non-critical commands to the addressed subsystem, performs attitude determination and control, collects and processes instrument data, sequences downlink telemetry, and performs advanced autonomy algorithms for operations. An FPP evaluates the performance of the spacecraft by monitoring the data flow and content of the 1553 data bus. Its main function is to provide error correction and redundancy management. A low-power, 8-Gbit SSR card, using Reed–Solomon error-correcting code, stores data between ground contacts. A power-converter card provides regulated power to the cards within the IEM.

A redundant MIL-STD-1553 serial-data bus connects the IEMs with attitude sensors (the inertial measurement unit and star tracker), the remote interface unit (RIU), and the redundant instrument DPUs. A dedicated low-voltage, differential-signaling (LVDS) interface is used to collect images at high bit rates (not shown on Fig. 4). Finally, an RIU provides the interfaces between the redundant IEM units and the attitude components not on the 1553 data bus, i.e., the reaction wheels, Sun sensors, and solar-array drives.

Fault tolerance is achieved by box-level redundancy and careful interface design. The IEEE-1394 serial data bus between the IEMs is redundant. The 1394 bus between IEMs allows the data connections to be effectively cross-strapped between all cards in both IEM chassis. Power distribution within the IEM is also an important factor in achieving fault tolerance. The FPP card and interface card in both IEMs are always powered and cannot be switched off. Failure of one of these resources is not fatal, since its backup will continue proper operation. The remaining boards are on switched

power and have their own dedicated power converter. During normal operations, one IEM is fully powered and designated as prime. The prime IEM is the 1553 bus controller and is responsible for all spacecraft functions. If a failure in the prime IEM is detected, by one or both FPPs, the other IEM is fully powered and designated as the new prime.

### 3.7. Command and data handling

The command and data handling (C&DH) subsystem is implemented by resources within the IEMs. The functions provided by the C&DH subsystem are command management, telemetry management, and time distribution.

The command function operates on cross-strapped inputs from the two command receivers at one of four rates: 500, 125, 31.25 bps (normal modes) or 7.8 bps (emergency rate). The format of the uplinked commands is CCSDS compliant, with a separate virtual channel for each side of the redundant C&DH subsystem. Commands can be executed in real time or can be stored for later execution. Execution of stored commands can be triggered by reaching a specific mission elapsed time or by the detection of a spacecraft event.

The telemetry function collects engineering status and science data for recording and downlink. Engineering data are collected by very small remote interface chips that accumulate analog telemetry information and relay it to the PDU over a serial inter-integrated circuit ($I^2C$) data bus. Other housekeeping data types are sampled by the RIU and PDU. These data and engineering data from other remote terminals are transferred to the IEM over the 1553 bus. Science data are collected over dedicated serial interfaces and the 1553 bus. Recorded data are read back and placed into the downlink on command. Recorder playback data can be interleaved with real-time data on the downlink, and data can be recorded on one of the redundant recorders while the other recorder is in playback.

The downlink data rate is selectable to match the downlink capability throughout the mission. While the C&DH subsystem controls the rate of production of real-time data packets to match the real-time downlink rate, the rate at which data are placed on the recorder is under the control of the subsystems. Each remote terminal on the 1553 bus can request the C&DH to pick up and record a variable number of bits of data per second, up to a maximum rate. This feature allows the spacecraft operators complete flexibility with respect to the bandwidth used by each instrument and spacecraft subsystem.

Spacecraft time is maintained by an oven-controlled oscillator inside the prime IEM that has frequency–temperature stability of $5 \times 10^{-8}$ over the expected spacecraft operating temperature range. Spacecraft time is synchronized between IEMs and delivered to the instruments over the 1553 data bus. Spacecraft time correlation to universal time is accomplished on the ground by comparing DSN time-tagged telemetry frames to spacecraft time within the frame.

### 3.8. Guidance and control

The guidance and control (G&C) subsystem is composed of a suite of sensors for attitude determination, actuators for attitude corrections, and algorithms that are executed in the main processor within the IEM to provide for continuous, closed-loop attitude control. No science instrument data are used for attitude determination or control. This subsystem is a logical duplicate of the NEAR Shoemaker attitude system (Strikwerda et al., 1998).

In operational mode, the attitude is controlled to a commanded pointing scenario. In safe modes, the G&C maintains the sunshade at the Sun and places the Earth within the medium-gain antenna pattern to establish ground communications. The G&C subsystem also controls the thrusters for $\Delta V$ maneuvers and for momentum management. Finally, the G&C subsystem controls the solar array drives to maintain the correct solar incidence angle for power production and panel temperatures.

The G&C sensor suite is composed of a redundant inertial measurement unit (IMU), two star trackers, five Sun sensors, and two Sun-sensor electronics units. The IMU, a key component of the G&C, contains redundant gyros and accelerometers aligned such that any three are sufficient for three-axis rate or acceleration measurement. Thus a single failure of a gyro or accelerometer can be tolerated. In addition, the IMU contains block-redundant power supplies and processing electronics. Normally, only three gyros are powered. Three of the accelerometers are powered approximately 24 h before each $\Delta V$ maneuver to allow for thermal stabilization and are turned off shortly after the maneuver.

The baseline star trackers are block redundant. Normally, only one star tracker is powered. The baseline Sun sensors are a version of a digital solar aspect detector (DSAD) modified for thermal protection and isolation. Five sensors and redundant sensor-electronics units are used. Four of the DSAD heads, each with a field-of-view of $130^\circ$, are mounted to look through the sunshade, with a field-of-view overlap of $20^\circ$. The dual electronics packages provide not only physical redundancy but also the ability to read solar position from two heads simultaneously for consistency checks. A fifth DSAD head is mounted on the back of the spacecraft and provides partial coverage in the opposite hemisphere to aid in recovery from emergencies. Combining the fields of view of the five Sun sensors yields 99% of full omnidirectional coverage. During normal and safe-mode operations both DSAD electronics and all five of the sensors are powered and used for fault protection.

The primary attitude sensors are the redundant star tracker and the redundant IMU. The star tracker operates at 5 Hz and is the primary absolute inertial reference. Differential measurements of attitude at 100 Hz are provided by the IMU's gyros. Measurements from these systems are combined in the attitude-determination filter, a recursive estimator operating continually in the IEM main processor. It provides knowledge of fiducial frame attitude to approximately

250 μrad about the star tracker boresight and approximately 35 μrad about the transverse axes. In addition to attitude and rate, the attitude determination filter estimates and compensates for gyro drift rates, thus greatly reducing the sensitivity of attitude accuracy to transient dropouts or blinding of the star tracker.

The attitude control actuators are the four reaction wheels and the propulsion system's small thrusters. During normal mission operations, all four wheels are powered and act as the primary attitude actuators. The wheels are arranged in a symmetric splayed configuration to provide redundancy in the event of any wheel failure and provide for symmetric "null-space torquing" in wheel speed and momentum management. The thrusters are used for attitude control during trajectory correction maneuvers, for momentum management (as required), and for emergency attitude corrections.

The outputs of the attitude sensor suite are processed at 1 Hz to provide a filtered estimate of the spacecraft state. These outputs are propagated in 20-ms steps until the next 1 Hz update. A desired state is computed from the commanded pointing scenario, which may be specified in an inertial or Mercury-centered coordinate system, using uploaded ephemerides of the Earth, Sun, Mercury, and the spacecraft. Control outputs are generated every 20 ms (50 Hz) to null the difference between the observed state and the commanded state.

During $\Delta V$ maneuvers, control of thruster firings and the related attitude control is implemented within the 50 Hz loop. Linear velocity is determined by direct integration of IMU accelerometer outputs. To ensure that accelerometer outputs are sufficiently accurate to meet trajectory $\Delta V$ precision requirements, individual accelerometer output biases are estimated via long-term, very-low-pass filtering of individual accelerometer data immediately prior to the burn.

Throughout the mission, solar radiation pressure produces an external force on the spacecraft. This force, if not acting through the spacecraft center-of-mass, results in an external torque. Over time, this torque builds system momentum. The magnitude and direction of the system momentum vector is a function of the solar intensity, spacecraft surface properties, and offset between the force vector and the center-of-mass. Normally this momentum is captured by changing the rotation speed of the reaction wheels. If, however, this effect is not eventually countered, the wheel speed will increase to a point where a thruster firing is required to lower system momentum and preserve control authority. Frequent momentum dumps via thrusters are undesirable; they are expensive for mission operations to schedule, test, and execute, and they can compromise science requirements for orbit determination accuracy. A non-propulsive momentum management technique using solar radiation pressure is planned to reduce greatly the number of momentum dumps. This technique has been successfully demonstrated on NEAR Shoemaker, where the spacecraft went over 30 months between thruster-based desaturation events (Lee and Santo, 1998). The G&C on-board software autonomously adjusts the spacecraft attitude, within predefined limits, using solar radiation pressure to produce opposing torques that reduce the system momentum. Preliminary studies indicate that this technique can effectively constrain the momentum buildup to a point where no momentum dumps are expected during the cruise phase, and momentum dumps are needed only once every four days during the orbit phase.

### 3.9. Flight software

The IEM software operates in the main processor (MP) and the fault-protection processor (FPP). Both MESSENGER processors share a common overall architecture for task interfaces and resource use that prevents deadlock and decouples unrelated processes. Other common codes have been identified. Using common software on both processors will reduce the areas of software development and test time.

The CPU margin of the two processors is estimated to be greater than 50%. The timing of baseline tasks for each processor has been estimated using adjustments to benchmarks and algorithms measured on similar hardware. Estimates of the program and large-data-structure memory requirements yield greater than 50% memory margin. None of the baseline tasks stretch the memory capacity of the processor design. The memory is sized to hold more than one copy of the applications program, to facilitate reprogramming.

To implement autonomous functions for safing in the FPP and operations in the MP, execution of command sequences stored on board can be triggered at a specified time or when a specific event occurs. Both processors will use the same rule-based autonomy architecture for this function. The use of table-driven rules and stored command sequences eliminates the need for much special-purpose "autonomy software" and decouples the autonomy algorithms from the software development. Both the command processing and rule-based autonomy designs will be minor extensions of the designs used on NEAR Shoemaker (Stott et al., 1998), where the designs have proven powerful and flexible, yet predictable in operation.

The MP will provide considerable autonomous operational capability in carrying out its functions. Guidance algorithms use spacecraft, Mercury, and Earth orbit knowledge to maintain a continuous picture of how the spacecraft is oriented with respect to the Sun, Earth, and Mercury. The MESSENGER guidance functions include autonomous imager scan mirror positioning, phased-array antenna pointing at Earth, solar-array rotation control, and event-based triggering for data collection and other tasks. These extended capabilities will greatly simplify mission operations, by allowing the use of very high-level commanding, such as "take an image at Mercury latitude $= X$, longitude $= Y$". The passive solar-pressure momentum management is carried out autonomously, in the same manner as on NEAR Shoemaker (Lee and Santo, 1998). In addition, the MP can implement autonomous power management, such that commanded data

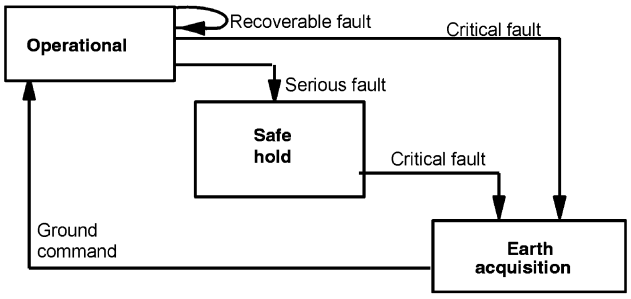


Fig. 16. The state transition diagram is simple and robust. Limiting the number of spacecraft modes greatly reduces test time and enhances system reliability. MESSENGER employs the same fault-protection modes as have been used with a great deal of success on the NEAR Shoemaker project (Lee and Santo, 1996).

collection tasks will be shut down (and associated loads shed) in a priority order, if the spacecraft power is insufficient to carry out all tasks during Mercury hot-spot transits. This capability allows the maximum possible data to be taken, given the solar array constraints, without taxing the mission operations planning capabilities.

The MP will implement a file system on the SSR, so that data from each instrument and data collection episode can be randomly accessed. This capability allows the MP to record data quickly during data collection episodes, retrieve selected data for compression during quiet periods, and rewrite the compressed data to the recorder for later downlink. A benchmark of lossless fast compression and 6-to-1 wavelet transform compression indicates background compression of a 12-Mbit image will take less than 5 min. This processing speed is more than sufficient to compress hundreds of images before downlink during the orbit phase.

### 3.10. Fault protection

In common with other interplanetary spacecraft, MESSENGER will spend long periods of time out of ground contact. MESSENGER has solar conjunction periods of up to 11 days where design for unattended operation is necessary. Even during ground contacts, the speed of light limits usefulness of real-time telemetry and commanding. Under these conditions, autonomous detection and correction of faults is a key area of spacecraft design. The goals of the fault protection design are to detect health-threatening faults and to keep the spacecraft safe until the next ground contact. Fault diagnosis and correction (beyond that needed to keep the spacecraft safe until the next ground contact) are functions of the ground-based mission operations team.

The operating-mode state-transition diagram is depicted in Fig. 16. It is a design similar to that employed on NEAR Shoemaker (Lee and Santo, 1996). Recoverable faults are handled in Operational Mode. An example of a recoverable fault is an anomaly in a non-critical subsystem, such as an instrument. For a recoverable fault, the offending component is turned off and the spacecraft remains in Operational Mode. Any serious fault affecting a critical spacecraft subsystem results in remedial action (such as bringing a backup system on-line) and entry into safe hold mode. In safe hold mode, the sunshade is pointed at the Sun and an MGA is pointed at Earth. Safe hold mode requires inertial reference. The Earth acquisition mode is the lowest safing mode. It is entered if the fault causes the G&C subsystem to lose inertial reference, for example, when switching between redundant MPs. Earth acquisition mode recovery is accomplished with the fanbeam pattern of the MGAs using a similar technique as that pioneered on NEAR Shoemaker (Bokulic and Jensen, 2000). When in Earth acquisition mode the sunshade is pointed at the Sun and the spacecraft is rotated about the Sun line at $2^{\circ}$ per minute. Once per revolution, an MGA output sweeps past the Earth, and a beacon signal is detected on the ground. After observing this signal sweep several times, a command is timed to intercept and stop the rotating spacecraft when the MGA is Earth pointing.

For either safe hold or Earth acquisition modes the spacecraft telecommunication and power configurations are set according to a reprogrammable table stored in non-volatile memory that turns off instruments and other non-critical subsystems, while powering all of the necessary systems (such as the backup star tracker) that may be used for recovery. The table selects the MGA and LGA that are currently facing Earth. Uplink communications are received through both an MGA and an LGA. If an extended period with no ground communications occurs, the antenna configurations are switched autonomously in a round-robin fashion.

The most critical aspect of spacecraft safety is maintaining a safe thermal environment. Most importantly, the sunshade must be between the spacecraft and the Sun. Secondly, the heat-sensitive top deck of the spacecraft must not be exposed to a large thermal input from the sunlit side of Mercury. (In normal operations, the top deck never views the hot planet at close distances.) Finally, the solar incidence angle on the arrays must be controlled to limit the maximum cell temperature.

Recovery from safe hold or Earth acquisition mode is straightforward. Using data transmitted at the emergency rate, the on-board problem is diagnosed and corrected by mission operations. The spacecraft can then be commanded to operational mode; only ground command can promote to operational mode. The spacecraft has extensive facilities for diagnostics of on-board problems, including a command history buffer, an autonomy history buffer, an attitude history buffer, snapshots of spacecraft data when the safe mode was entered, and a data summary area that records time-tagged high and low values of each piece of spacecraft housekeeping data.

### 3.11. Communications approach

The first scheduled DSN contact is approximately 78 min after MESSENGER's launch. The front and back LGAs

are connected to the redundant transponders to yield effective omnidirectional coverage at that time. Twenty-four-hour DSN coverage is scheduled for the first 5 days. Uplink during all nominal contacts is at least 31.25 bps; downlink during early operations is $>$ 1000 bps. DSN coverage is gradually reduced as initial instrument calibrations are completed and confidence is gained in spacecraft performance. The uplink and downlink designs are fully CCSDS-compatible.

Cruise phase is designed to minimize operations support except for short periods of intense activity around the flybys. Typical DSN coverage is two 8-h passes per week using the 34-m DSN antennas. The spacecraft antenna configuration is chosen so that all critical mission events are monitored with real-time telemetry. Normally, uplink communications are accomplished through the MGAs and downlink communications are accomplished through the phased-array antennas.

During the orbital phase, one 8-h 34-m DSN pass is scheduled daily, with 1 h of each pass allocated for DSN setup. Doppler tracking and occasional ranging are used to satisfy navigation and science requirements.

Emergency communications are accomplished through the LGAs and MGAs. Uplink is at 7.8 bps and downlink is at 10 bps. The antenna configuration supports an LGA uplink and an MGA downlink over the entire mission using the 70-m DSN antennas while maintaining sunshade attitude requirements and 3 dB link margins.

During both cruise and orbital operations, periods of solar conjunction preclude communications. Prior to these times, the spacecraft is placed into a safe-hold mode. No events requiring ground commands occur during solar conjunction periods.

## 4. Conclusion

Orbiting Mercury is a challenging task. The MESSENGER mission design utilizes a Delta II launch vehicle and a chemical-propulsion spacecraft to deliver up to 476 kg of dry mass into Mercury orbit. A preliminary spacecraft design has been completed that gives confidence that this mass target can be achieved and that the thermal problems of the Mercury environment can be solved using standard space-grade electronics.

The project is currently in the preliminary design phase, during which system-level trade studies are being investigated to improve performance and/or reduce implementation risk. Examples of active studies include switching to a Ka-band downlink with the phased-array antennas to improve science data-rate return, lengthening the sunshade to increase orbital-phase science viewing opportunities, increasing the mass of the reaction wheels to reduce the frequency of momentum-dump thruster firings to improve orbit determination, and adding phase-change material to some of the instruments to reduce their temperature transients during the hot-planet crossings. The trade studies will be completed before the preliminary design review in May 2001, which initiates the transition to the detailed design phase. Other project milestones include the critical design review in March 2002, the start of integration and test in November 2002, and the shipment to the launch site in December 2003.

The mission and spacecraft designs combine generous margins with appropriate technologies to define a low-cost, low-risk Mercury orbiter implementation. These systems, combined with a diverse suite of instruments (Gold et al., 2001), can accomplish all scientific objectives (Solomon et al., 2001) for the mission.

## Acknowledgements

We thank Barbara Northrop for assistance with manuscript preparation. The MESSENGER mission is supported by the NASA Discovery Program under contracts to the Carnegie Institution of Washington (NASW-00002) and The Johns Hopkins University Applied Physics Laboratory (NAS5-97271).

## References

Bokulic, R.S., Flaherty, M.K.E., Jensen, J.R., McKnight, T.R., 1998. The NEAR spacecraft RF telecommunications system. Johns Hopkins APL Technical Digest 19 (2), 213–219.

Bokulic, R.S., Jensen, R.R., 2000. Recovery of a spacecraft from Sun-safe mode using a fanbeam antenna. J. Spacecraft Rockets 37 (6), 822–826.

Dakermanji, G., Butler, M., Carlsson, P.U., Temkin, D., 1998. The TIMED spacecraft power subsystem design. Fifth European Space Power Conference, European Space Agency (ESA), Tarragon, Spain, ESA SP-416, September 21–25, 447–453.

Dunne, J.A., Burgess, E., 1978. The Voyage of Mariner 10: Mission to Venus and Mercury. NASA SP-424, NASA Scientific and Technical Information Office, Washington, DC, 124 pp.

Ercol, C.J., Jenkins, J.E., Dakermanji, G., Santo, A.G., Mason, L.S., 2000. Prototype solar panel development and testing for a Mercury orbiter spacecraft, 35th Intersociety Energy Conversion Engineering Conference, American Institute of Aeronautics and Astronautics, Paper AIAA-2000-2881, Las Vegas, NV, July 24–28, 11 pp.

Gold, R.E., Solomon, S.C., McNutt, Jr., R.L., Santo, A.G., Abshire, A.B., Acuña, M.H., Afzal, R.S., Anderson, B.J., Andrews, G.B., Bedini, P.D., Cain, J., Cheng, A.F., Evans., L.G., Follas, R.B., Gloeckler, G., Goldsten, J.O., Hawkins, III, S.E., Izenberg, N.R., Jaskulek, S.E., Ketchum, E., Lankton, M.R., Lohr, D.A., Mauk, B.H., McClintock, W.E., Murchie, S.L., Schlemm, II, C.E., Smith, D.E., Starr, R.D., Zurbuchen, T.H., 2001. The MESSENGER mission to Mercury: scientific payload. Planet. Space Sci., this issue.

Lee, S.C., Santo, A.G., 1996. Near Earth Asteroid Rendezvous (NEAR) spacecraft safing design. Acta Astron. 39, 197–206.

Lee, S.C., Santo, A.G., 1998. In: Wertz, J.R. (Ed.), Reducing mission operations costs through spacecraft autonomy: the Near Earth Asteroid Rendezvous (NEAR) experience. Kluwer Academic Publishers, Dordrecht. J. Reducing Space Mission Cost 1, pp. 87–104.

Mason, L., 1999. High flux, solar vacuum testing of a solar array panel and heat shield. NASA John E. Glenn Research Center at Lewis Field Report, February.

McAdams, J., Horsewood, J., Yen, C., 1998. Discovery-class Mercury orbiter trajectory design for the 2005 launch opportunity. American Aeronautical Society/American Institute of Aeronautics

and Astronautics (AAS/AIAA) Astrodynamics Specialist Conference, AIAA 98-4283, August.

Mosher, L.E, Wiley, S., 1998. Design, development, and flight of the NEAR propulsion system. Johns Hopkins APL Technical Digest 19 (2), 174–184.

NASA, 1997. The Space Science Enterprise Strategic Plan, Origin, Evolution, and Destiny of the Cosmos and Life. 41 pp.

Rayman, M., Lehman, D., 1997. Deep Space One: NASA's first deep space technology validation mission. 48th International Astronauical Congress, Turin, Italy, October 6–10.

Roadmap Development Team, 1998. Mission to the Solar System: Exploration and Discovery, A Mission and Technology Roadmap. Gulkis, S., Stetson, D.S., Stofan, E.R. (Eds.). Jet Propulsion Laboratory, Pub. 97-12.

Santo, A.G., Lee, S.C., Gold, R.E., 1995. NEAR spacecraft and instrumentation. J. Astron. Sci. 43 (4), 373–397.

Solomon, S.C., McNutt, Jr., R.L., Gold, R.E., Acuña, M.H., Baker, D.N., Boynton, W.V., Chapman, C.R., Cheng, A.F., Gloeckler, G., Head, III, J.W., Krimigis, S.M., McClintock, W.E., Murchie, S.L., Peale, S.J., Phillips, R.J., Robinson, M.S., Slavin, J.A., Smith, D.E., Strom, R.G., Trombka, J.I., Zuber, M.T., 2001. The MESSENGER mission to Mercury: scientific objectives and implementation. Planet. Space Sci., this issue.

Stott, D.D., Artis, D.A., Heggestad, B.K., Kroutil, J.E., Krueger, R.O., Linstrom, L.A., Perschy, J.A., Schwartz, P.D., Sweitzer, G.F., 1998. The NEAR command and data handling system. Johns Hopkins APL Technical Digest 19 (2), 220–233.

Strikwerda, T.E., Ray, J.C., Haley, D.R., 1998. The NEAR guidance and control system. Johns Hopkins APL Technical Digest 19 (2), 205–212.

Wertz, J.R. (Ed.), 1978. Spacecraft Attitude Determination and Control, Appendix L, Solar system constants. Kluwer Academic Publishers, Dordrecht/Boston/London, pp. 814–825.

Yen, C.-W., 1985. Ballistic Mercury orbiter mission via Venus and Mercury gravity assists. Proc. American Aeronautical Society/American Institute of Aeronautics and Astronautics (AAS/AIAA) Astrodynamics Specialist Conference, AIAA No. 85-346, San Diego, CA.

Yen, C.-W., 1989. Ballistic Mercury orbiter mission via Venus and Mercury gravity assists. J. Astron. Sci. 37, 417–432.